IEEE Access
Multidisciplinary | Rapid Review | Open Access Journal

Received January 24, 2020, accepted February 17, 2020, date of publication March 20, 2020, date of current version March 31, 2020.

Digital Object Identifier 10.1109/ACCESS.2020.2982247

WBAN Channel Characteristics Between Capsule Endoscope and Receiving Directive UWB On-Body Antennas

MARIELLA SÄRESTÖNIEMI[1], CARLOS POMALAZA-RÁEZ[2], (Senior Member, IEEE), CHAÏMAÂ KISSI[3], MARKUS BERG[1], MATTI HÄMÄLÄINEN[1], (Senior Member, IEEE), AND JARI IINATTI[1], (Senior Member, IEEE)

[1]Centre for Wireless Communications, Faculty of Information Technology and Electrical Engineering, University of Oulu, 90570 Oulu, Finland
[2]Department of Electrical and Computer Engineering, Purdue University at Fort Wayne, Fort Wayne, IN 46805, USA
[3]Electronics and Telecommunication Systems Research Group, National School of Applied Sciences (ENSA), Ibn Tofail University, Kenitra 14000, Morocco

Corresponding author: Mariella Särestöniemi (mariella.sarestoniemi@oulu.fi)

This work was supported in part by the Projects WBAN Communications in the Congested Environments (MeCCE), the Academy of Finland 6Genesis Flagship, under Grant 318927, and in part by the European Union's Horizon 2020 Programme through the Marie Sklodowska-Curie under Grant 872752.

ABSTRACT This paper presents a study on the ultra wideband (UWB) radio channel characteristics between a capsule endoscope and a directive on-body antenna in different parts of the small intestine. The study is conducted using a finite integration technique (FIT) based electromagnetic simulation software CST Studio Suite and four of its anatomical voxel models. The capsule endoscope model is set inside different areas of the small intestine of the voxel models. A recently published directive on-body antenna designed for in-body communications is used in the evaluations. The obtained frequency and time domain channel characteristics are compared with previously published results with another directive on-body antenna designed for capsule endoscopy communications. Power flow presentations are used to understand differences obtained with two on-body antennas. Different rotation angles of the capsule are also considered in this study. It is found that channel characteristics vary remarkably depending on the antenna location in the small intestine and location of the on-body antenna. Thus, the on-body antennas should be located carefully to ensure coverage over the whole intestine area. Path loss does not only depend on the distance between a capsule and the on-body antenna but also on the tissues between the capsule and on-body antennas. Obviously, the antenna patterns have clear impact on the received signal's strength. Furthermore, orientation of the capsule affects also strongly impact when linearly polarized antennas are used.

INDEX TERMS Abdominal monitoring, capsule endoscopy, directive antenna, ultrawide band, wireless body area networks.

I. INTRODUCTION

Capsule endoscopy has brought strong interest in recent years due to several advantages it offers for the examination of the gastrointestinal tract (GI). It is reliable, painless, and comfortable way to examine especially the small intestine (SI) area, which is not easily reached with the conventional endoscopy techniques. In the capsule endoscopy, the patient just swallows a small pill, which contains a camera and transmitter, and wears a monitoring device on the waist where the data from the capsule is recorded [1]–[4].

Different techniques are used to transmit data from a capsule to an on-body device. Ultra wideband (UWB) has recently become an attractive alternative for the communication technology since it enables reliable and high-data rate data transfer with low power consumption and simple electronics. Besides, its large bandwidth enables high resolution for the images [5]. The frequency bandwidth determined by the IEEE 802.15.6 standard for UWB Wireless Body Area Networks (WBAN) [7] is 3.1 – 10.6 GHz. The propagation losses in the tissues increase as the frequency increases.

The associate editor coordinating the review of this manuscript and approving it for publication was Lorenzo Mucchi.

Thus, the lower part of the UWB band is usually considered for the capsule endoscopy application [5], [6].

Smooth design of transceivers requires deep knowledge of the channel characteristics and propagation within the tissues. Thus, there are several WBAN channel models and propagation studies presented in the literature for wearable and implant communication systems in the human abdomen area [5], [6], [8]–[18]. Furthermore, the research in antenna design, both for capsule antennas as well as for on-body receiver antennas, has been active recently [19]–[28]. Channel characteristics between the capsule antenna and on-body antenna is studied, e.g., in [5], [6], [19]. In-body power distribution in the abdominal area was studied in more details in [18]. It was shown that the power inside the abdomen area is distributed depending on the tissues and antenna locations. Even the challenging locations in the small intestine area can be reached with appropriate on-body antenna locations. In [18], two different on-body antennas were considered in the evaluations, the first one was introduced in [26] and the second one in [27]. Initial channel characteristics evaluations between the capsule endoscope and the on-body antenna were performed in [18].

A deeper study on the channel characteristics between endoscope capsule and on-body antenna [26] with an anatomical voxel model was presented in [11]. The study covers different parts of the voxel model's small intestine as well as layer model evaluations. Impact of the rotation angle is studied as well.

This paper presents an extensive signal propagation evaluation study with the on-body antenna introduced in [27]. The study covers frequency and time domain cannel results with several on-body and capsule locations as well as results with different voxels models. Furthermore, 2D power flow presentations are studied in more details to understand how the signal propagates from the capsule. An impact of the rotation angle of the capsule studied as well. The paper compares the results with capsule-on-body antenna channel evaluations presented in [19] using an on-body antenna introduced in [26].

Novelty of this research is that there are only few papers presenting capsule – on-body antenna UWB-WBAN channel characteristics using realistic directive on-body antennas. Furthermore, up to author's knowledge, there are no other studies presenting capsule-channel evaluation results with several voxel models having different sizes and body constitutions.

The paper is organized as follows: Section II describes the study case, i.e., voxel models used in the simulations, capsule model and capsule locations, as well as the on-body antennas and antenna locations. Section III presents the results for channel characteristics between the endoscope capsule and on-body antenna with different antenna locations. Section IV presents the channel characteristics with different voxel models. Section V presents the impact of the capsule's rotation angles on the channel characteristics. Conclusions are given in Section VI.

II. STUDY CASE

This section explains details of the study case: simulation models, the on-body antenna, antenna locations, capsule model and capsule locations.

A. VOXEL MODELS

In this study, the simulations were conducted using the 3D electromagnetic simulation tool CST MicroWaveStudio [29], which is based on the finite integration technique (FIT). The basic idea of FIT is to calculate the radio propagation by solving the Maxwell's equations in their integral form. Details of the FIT can be found, e.g., in [30].

In the simulations, we used two female and two male voxel models, which are presented in Fig. 1. The first female voxel is Laura, which models a young lean female body. The resolution of Laura voxel is 1.88 mm × 1.88 mm × 1.88 mm. The second female voxel is Donna, which models a middle-aged overweight female. The resolution of Donna is 1.88 mm × 1.88 mm × 2 mm. The first male voxel is Gustav, which corresponds to the young, lean male body with the resolution of 2.08 mm × 2.08 mm × 2.08 mm. The second male voxel is Hugo, which models a middle-aged, overweight male body with the resolution of 1 mm × 1 mm × 1 mm. The lines, along which the cross-section is performed, are presented on the sides of the voxels. For Laura, Donna, and Hugo, the cross-section is performed on the navel area, since their small intestines are located on the front part of the abdomen. Instead for Gustav, who is taller than the other models, small intestine is located on the front part of the abdomen slightly above the navel area.

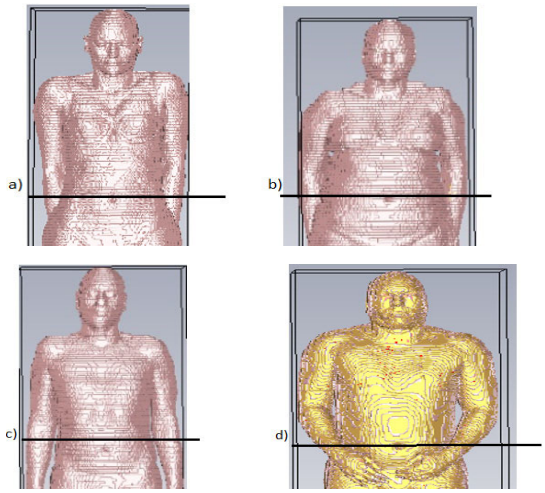

FIGURE 1. Anatomical voxel models a) Laura, b) Donna, c) Gustav, d) Hugo.

Cross-sections of these models are presented in Figs. 2a–d. As it is noted, there are clear differences in the structures of the intestine area between the models. Besides, thicknesses of the fat layers (both inner and outer) and muscle layer vary significantly between the models.

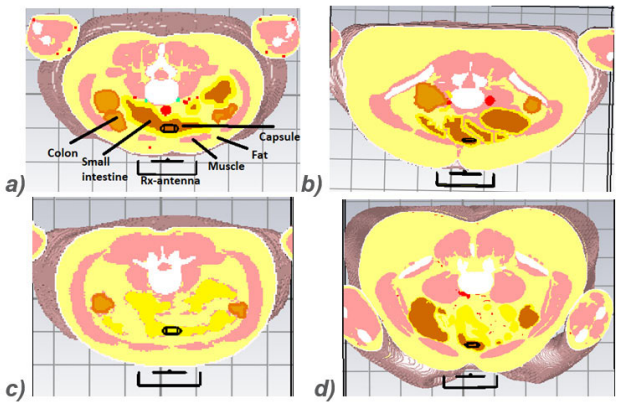

FIGURE 2. Cross-sections of the voxel models a) Laura, b) Donna, c) Gustav, d) Hugo.

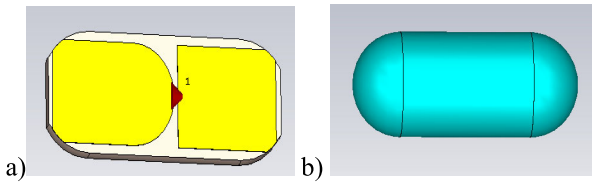

FIGURE 3. a) Dipole antenna inside the capsule, b) capsule shell.

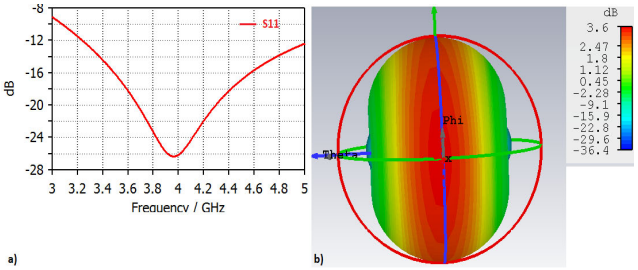

FIGURE 4. a) Reflection coefficient S11 of the capsule antenna, b) free-space radiation pattern of the capsule antenna.

B. CAPSULE ENDOSCOPE MODEL AND CAPSULE LOCATIONS

In this study, we use same simplified capsule model as in [18] and [19], where the details of the model can be found. This section only briefly summarizes the main characteristics of the model.

In the capsule model, an omnidirectional dipole antenna is embedded in plastic capsule shell, which has realistic dimensions: 11 mm × 25 mm, corresponding to the size of the commercial capsules nowadays [1]. The scheme of the dipole antenna and the capsule shell are presented in Fig. 3a–b, respectively. The dipole antenna is designed to work at the frequency of 4 GHz inside the small intestine. The reflection coefficient S11 and the radiation pattern of the dipole antenna are presented in Figs. 4a–b, respectively, [18].

Capsule is set in different parts of the voxel model's small intestine for the channel evaluations. The capsule locations are presented in Fig. 5 a–e.

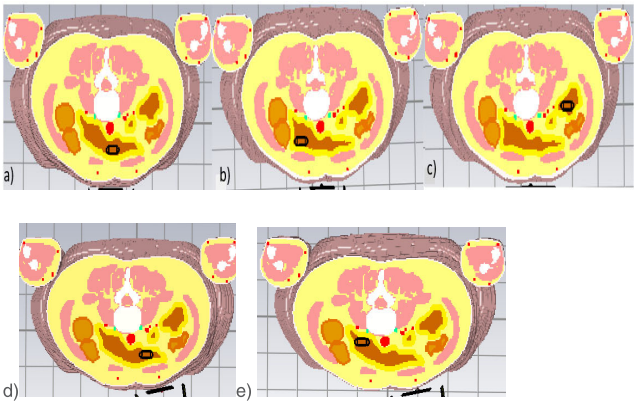

FIGURE 5. Capsule endoscope locations in Laura voxel model's small intestine: a) middle, b) left, and c) right, d) front right, and e) far left side of the small intestine.

C. ON-BODY RECEIVING ANTENNA AND ANTENNA LOCATIONS

In this study, we used a directive low-band UWB on-body antenna, which is designed for in-body communications. The antenna's radiator has a form of a ring, and thus it is referred to as a Ring antenna. The antenna has a cavity to enhance the directivity. The size of the cavity is (x=83 mm, y=49.5 mm, and z=19.62 mm, where z is towards the body. The design scheme and the radiation patterns of the antenna are illustrated in Figs. 6a–b. The antenna is designed to work at frequency band 3.75 – 4.25 GHz, which meets the IEEE 802.15.6 standards requirements [6]. The antenna is originally introduced in [27]. Detailed description of the antenna and its properties can be found in [27] and [28] and initial radio channel evaluation studies for capsule endoscope communications can be found in [18].

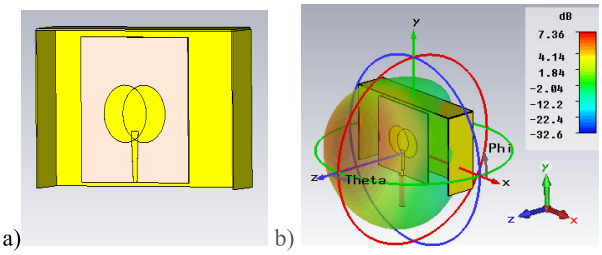

FIGURE 6. a) Scheme and b) free-space radiation pattern of Ring on-body antenna.

As a reference antenna, we use the on–body antenna designed for capsule endoscope communications introduced originally in [26]. The design scheme and the radiation patterns of the antenna are illustrated in Figs. 7a–b. The channel evaluations between the capsule endoscope and this reference on-body antenna are presented in [19]. The main difference between the Ring antenna and the reference antenna is in the sizes of the cavities. The size of the reference antenna is x=91mm, y=86 mm, and z=40.5 mm Besides, the structure of the reference antenna is different to the Ring antenna.

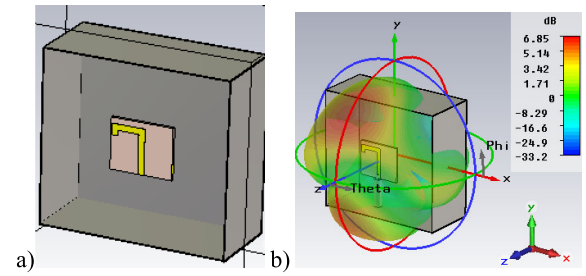

FIGURE 7. a) Scheme and b) free-space radiation pattern of the reference on-body antenna.

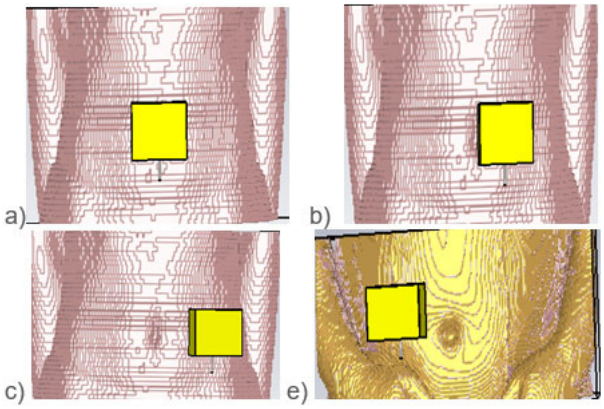

FIGURE 8. a) Antenna location 1, b) antenna location 2, c) antenna location 3, d) antenna location 4.

Details of the structures and dimensions of the antennas can be found in [27], and [26].

In this study, we used four different locations for the on-bodyi antenna as presented in Figs. 8a–d. Antenna location 1) is on the navel. As explained in [18], the advantage of locating antenna on the central line of the abdomen is that since there is no muscles on the central line, the part of the signal can travel towards intestine area without passing by the muscle layer, which is one of the most challenging tissues for the propagation due to its high relative permittivity [31]. Another advantage in this antenna location is that the navel provides additional air between the antenna and body surface, which is known to be beneficial for most of the antennas. [18]. In the antenna location 2, presented in Fig. 8b, the antenna is shifted 4 cm on the right side from the central line. The main advantage of this antenna location is that it covers the intestine area wider than the antenna location 1. However, the disadvantage is that the signal must pass through the muscle layer which causes more losses [18]. In the antenna location 3, the antenna is further shifted 4 cm on the right aiming to provides better view on the deepest parts of the small intestine. Antenna location 4, which is on the left side of the abdomen, is used for the voxels for which antenna locations 2 is not possible for the restrictions of the voxel model, as will be explained in Section IV. In all the antenna location cases, antenna-body distance is 4 mm [26].

III. POWER FLOW EVALUATIONS

This section presents 2D power flow presentations with Laura voxel model for the capsule and the on-body antennas separately. Aim of the power flow representation is to show how signal travels from the antenna taking into the account the antenna characteristics as well as the different tissues between the capsule and the on-body antenna. Details of the definition of the power flow representation can be found e.g. in [32]. Although in the capsule endoscopy communications, the capsule is the transmitter, this section presents power flow representations also from the on-body antenna, since it provides insight about the on-body antenna radiation characteristics. In addition, the radio channel is expected to be reciprocal. In this study, on-body antenna locations 1, 2, and 3 are considered. On-body antenna location 1 and capsule location "middle" is considered more in details for both on-body antennas from the viewpoints of horizontal and vertical cross-cuts. Antenna location 2 is evaluated for Ring antenna and reference antenna with the horizontal cross-cut. Antenna location 3 is evaluated only for the Ring antenna with horizontal cross-cut.

A. ANTENNA LOCATION 1

First, we consider antenna location 1 and capsule location "middle" with Ring antenna, as shown in Fig. 9a, which is the zoomed version of the horizontal in Fig. 5a. Power flow at 4 GHz is presented in Fig. 9b for the dB range of 0 – 70 dB, where 0 dB is set on the antenna. Power flow is noted to spread relatively smoothly from the capsule according to its radiation pattern presented in Fig. 4b. The flow is slightly weaker towards the body surface since the capsule is located in the vicinity of the outermost small intestine wall

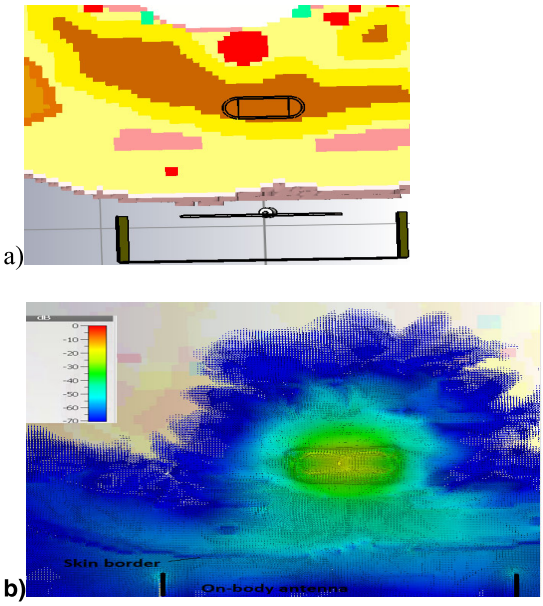

FIGURE 9. a) Horizontal cross-cut for case A, b) power flow at 4 GHz from the capsule with Ring antenna at antenna location 1.

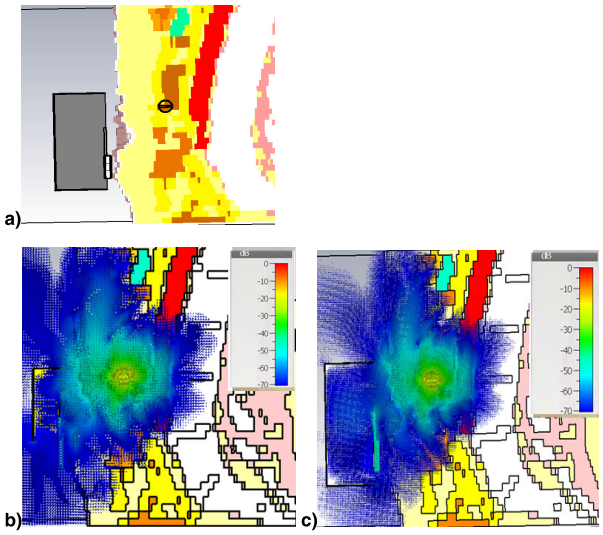

FIGURE 10. a) Vertical cross-cut for case A, b) power flow at 4 GHz from the capsule with Ring antenna, b) power flow from the capsule with reference antenna at antenna location 1.

and borders of the tissues with different dielectric properties, which cause diffractions on the propagating signal [30]. In the opposite direction, the small intestine wall is slightly further and thus, the power flow is stronger to that direction. When studying power flow (at 4 GHz) from the capsule towards the on-body antenna, it is noted that power flow is strongest through the central line of the abdomen and outer fat layer and less power can be seen in the muscle layers. This is evident from the results presented in [18], [20], [33], [34], which discuss about the fat as propagation medium.

Next, the power flow at is studied from the viewpoint of vertical cross-cut as presented in Fig. 10 a. Power flows at 4 GHz are presented separately for the Ring antenna and reference antenna in Figs. 10b–c, respectively. The reason for plotting the power flows separately for the antennas is to show the power flow on the edges of the cavities for both antennas, since the cavities have different sizes. It is noted that with these capsule and on-body antenna locations, the larger cavity size may provide benefit since the power flow level is reasonable still on the upper part of the reference antenna's cavity.

Next, we evaluate power flow from the on-body antenna to get insight of the on-body antenna's radiation characteristics. The power flows for horizontal cross-cut for the Ring and the reference antenna at 4 GHz are presented in Figs. 11a–b. Also, in this case, the plotted range is 0 – −70 dB. As it can be seen, power flow behavior is slightly different at this cross-cut level between the Ring and the reference antenna. The reference antenna has slightly stronger power flow towards the capsule. Besides, the power flow at higher dB levels is wider. This is natural since the reference antenna has a larger cavity. However, with both antennas, power flow at this range covers most of the intestine area. Only the rightmost part of the voxel model's intestine area is just partially covered.

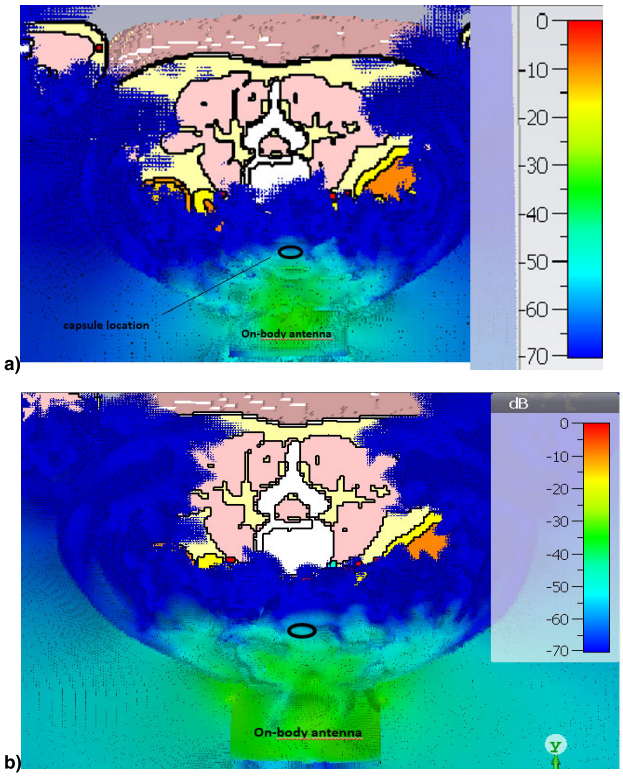

FIGURE 11. Power flow at 4 GHz from the a) Ring antenna and b) reference antenna at antenna location 1 in the selected horizontal cross-cut.

B. ANTENNA LOCATION 2

Figs. 12a–b presents power flow at 4 GHz with the Ring antenna and the reference antenna at the antenna location 2, respectively. Also, in these cases, plotted power flow range is 0 – −70 dB. The locations of the capsule are marked in the figures as well. In this case, there is remarkable difference between the Ring antenna and the reference antenna: within the plotted power flow range at this horizontal cross-cut level, almost the whole voxel model is covered except the most interior part of the body with the reference antenna. The intestine area is also covered expect small areas in which capsule location "left far" is included. Instead with the Ring antenna, intestine area is covered only partially. However, also in this case both capsule location "middle" and "right" are reached within this dB range.

IV. RADIO CHANNEL EVALUATIONS

This section presents radio channel characteristics in frequency domain and time domain for the transmitting capsule endoscope and the receiving on-body antenna in different parts of the small intestine with different on-body antenna and capsule locations. Frequency domain results are presented as frequency channel response S21, which is ratio of the received and the transmitted powers. Time domain results include presenting channel impulse responses, which are obtained using inverse fast Fourier transform (IFFT) for S21, for the whole simulated bandwidth 0 – 5 GHz. Both Ring

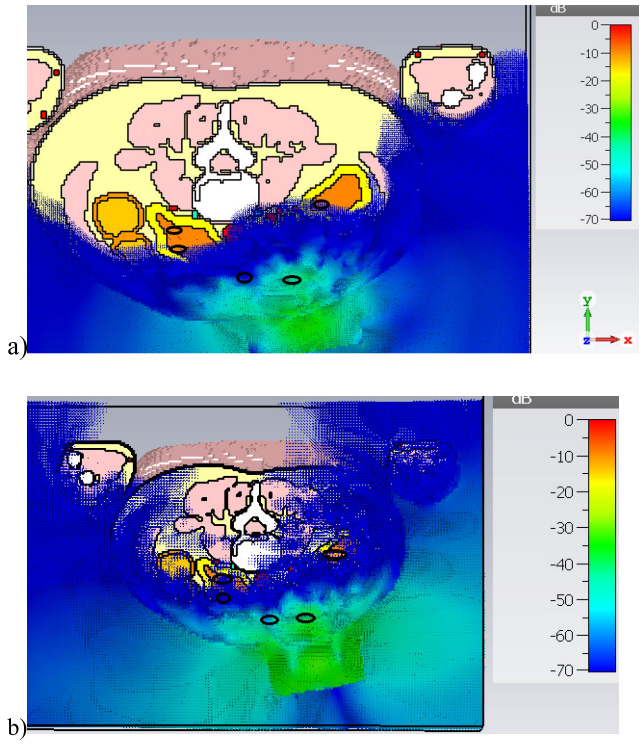

FIGURE 12. Power flow at 4 GHz from the capsule in the vertical cross-cut with a) Ring antenna, b) Reference antenna at antenna location 2.

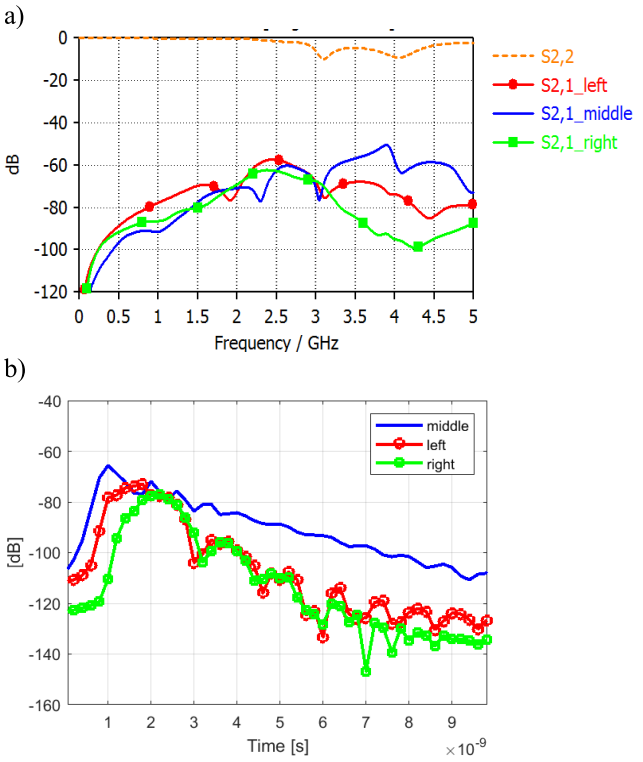

FIGURE 13. a) Frequency and b) time domain channel characteristics at the on-body antenna location 1 obtained with the Ring on-body antenna.

antenna and reference antenna are evaluated and compared for the antenna locations 1 and 2, only Ring antenna in the antenna location 3.

A. ON-BODY ANTENNA LOCATION 1

This subsection presents evaluations of the channel characteristic between the capsule and the on-body antenna as the on-body antenna is located on the navel (antenna location 1) and the capsule is located in the middle, left, and right sides of the small intestine.

The S21 value (in decibels) and impulse response in different capsule locations are presented for the Ring antenna in Figs. 13a–b, and for the reference antenna in Figs. 14a–b, respectively. S22s for the Ring and the reference antennas are also presented together with S21s results to describe the antenna matching. As it can be seen from Figs. 13a and 14a, antenna matching with the selected antenna body distance (4 mm) is weaker than in the free-space [26], [27], since there is a frequency shift with both antennas. However, the shift is clearly minor with the reference antenna. For these on-body antennas, the optimal antenna matching is obtained with antenna-body distance 30 mm, which however is not considerable for practical applications. Besides, in [16] it was found that although the antenna matching is weaker with antenna-body distance 4 mm, there are not significant differences in the propagation depths between the antenna-body distances 30 mm and 4 mm.

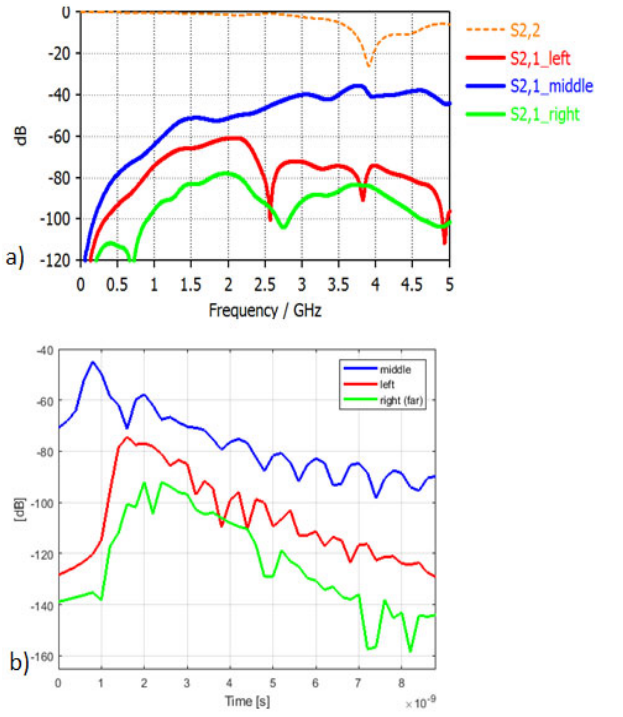

FIGURE 14. a) Frequency and b) time domain channel characteristics at the on-body antenna location 1 obtained with the reference antenna.

For the Ring antenna, within the frequency range of interest, i.e., 3.75 – 4.25 GHz, path loss is smallest, approximately 60 dB, as the capsule is located on the middle of SI. Although

the path loss is clearly smaller compared to the ''left'' and ''right'' cases, path loss in the capsule location ''middle'' is surprisingly high taking into the account that the physical distance between the capsule and the on-body antenna is so small. Besides, the part of the signal can travel from the capsule towards the on-body antenna via central line of the abdomen without passing the muscle layer. As a comparison, the path loss with the reference antenna in the capsule location ''middle'' is 40 dB, i.e., 20 dB smaller than that with the Ring.

The weaker antenna matching with Ring antenna is one explanation for the weaker S21. With this antenna location and antenna-body distance, the presence of the human body seems to cause a notch in Ring antenna's radiation pattern towards this capsule location in the middle of the SI. Details of the antenna radiation patterns for Ring antenna can be found in [27] and [28]. Power flow representation presented in Fig. 11 does not show any clear notch with the Ring antenna at the selected horizontal cross-cut level. Thus, we present the power flow plots from the viewpoint of the vertical cross-cuts with different levels. Figs. 15a1–c1 presents power flow at 4 GHz for Ring antenna with vertical cross-cuts for different cross-cut levels along the x-axis x=3, x=12, and x=24, which correspond to the left, middle, and right parts of the capsule. Figs. 14a2–c2 presents power flows with the same cross-cut levels with the reference antenna. The location of the capsule is marked as a circle in the figures. These figures illustrate clearer, why the channel between the capsule and the Ring antenna is weaker than that of the capsule and the reference antenna: In the case of reference antenna, the capsule is located in the vicinity of the green areas (higher power level), whereas in the case of the Ring antenna, the capsule is surrounded mostly by the blue (lowest power level) areas.

In the capsule location ''right'' the path loss is largest, approximately 95 dB, in the frequency range of interest with both on-body antennas, as presented in Fig. 13a and Fig.14a. This is obvious since the physical distance between the capsule and the on-body antenna is the largest. The path loss for the capsule location on the left part of SI are somewhere between the middle and right cases, approximately 75 dB, for the reference antenna slightly larger. It was interesting to note that with Ring antenna, path loss difference between ''right'' and ''left'' cases is significantly minor outside the frequency range of interest. Besides, path loss is relatively small, around 2.5 GHz although it is out of the antenna's operational frequency band. With the reference antenna, the variation between different cases is larger.

In time domain results, presented in Fig. 13b, we can see clear differences in the level, shape, and timing of the main peaks. However, the level differences are smaller than with the reference antenna, as shown in Fig. 14b. especially between the left and right cases. The differences in the timing of the main peaks are mostly due to the different distances between the capsule and the on-body antenna. The differences in the side peak can also be due to the different propagation velocities in different tissues [34]. The radiated

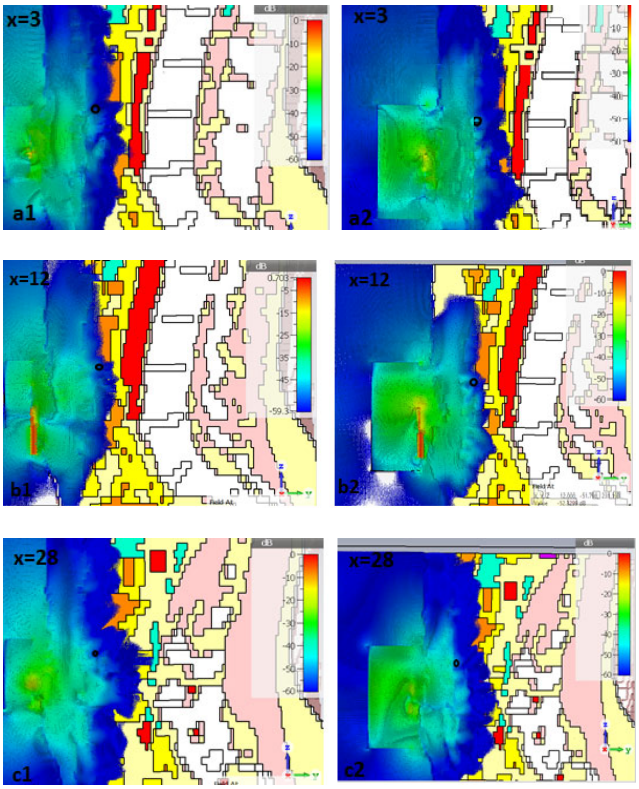

FIGURE 15. Power flow at 4 GHz from the capsule in different vertical cross-cuts for Ring antenna in a1–c1 and for reference antenna in a2–c2.

power is rather widely spread in time, which indicates that electromagnetic wave diffracting at the borders of different tissues as well as within the tissues due to the different dielectric properties of the tissues.

With a brief inspection, the reference antenna appears to be significantly better antenna for the capsule communications since the power flow coverage appears to be wider (at least in the studied cross-cut levels) and the channel impulse response between the on-body antenna and the capsule located in the ''middle'' is very strong. However, as we evaluate the channel for all these different capsule locations, we notice that only in Ring antenna's case each of these three impulse responses achieves the level of −85 dB, which is often considered as a minimum requirement for the signal detection. With the reference antenna, the weakest channel's main peak is at the level of −95 dB. Hence, it can be concluded that Ring antenna at the antenna location 1 would be suitable for detecting the data transmitted from the capsule in all these capsule locations whereas reference antenna could detect on the capsule locations ''middle and ''left''. The result is positive since it means that reasonable channels can be obtained with smaller cavity sizes as well.

B. ANTENNA LOCATION 2

Next, the channel characteristics are evaluated in the on-body antenna location 2, where the on-body antenna is transferred towards right from the navel. Firstly, the antenna matching

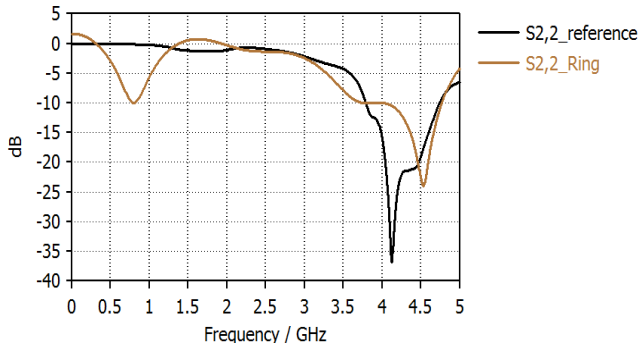

FIGURE 16. S22s for the Ring antenna and reference antenna.

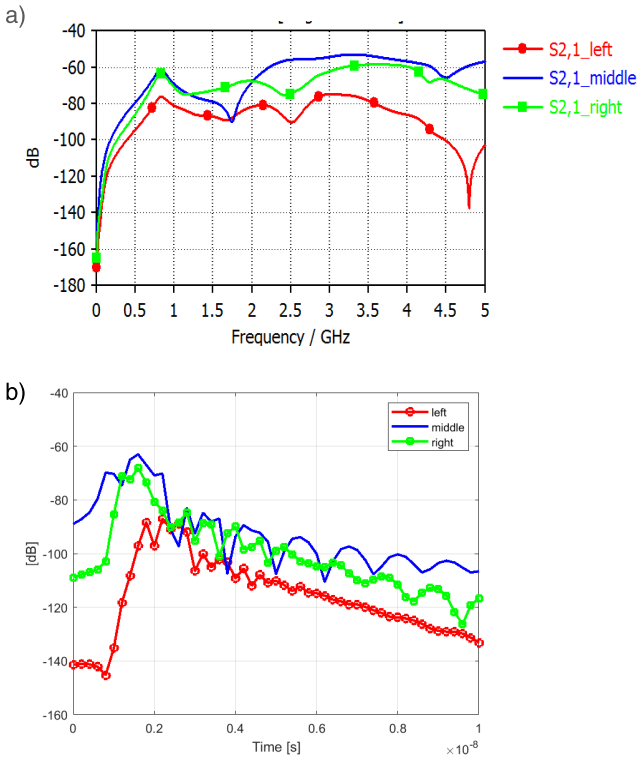

FIGURE 17. a) Frequency and b) time domain channel characteristics at the on-body antenna location 1 obtained with the Ring antenna.

is compared between the antennas. S22 for the Ring and the reference antenna are presented in Fig. 16. As one can note, antenna matching is weak with Ring antenna also in this case having a frequency shift of 0.5 GHz. However, the matching is better than in the antenna location 1. Reference antenna has a frequency shift as well though much minor than the Ring antenna. The frequency and time domain channel characteristics are presented for the Ring antenna and the reference antenna in Figs. 17a–b and 18a–b, respectively. In the case of Ring antenna, the path losses in the capsule locations "right" and "middle" are almost the same within the frequency range of interest, slightly less than 60 dB. Instead, the path loss in the capsule location "left" is significantly larger, almost −85 dB.

From cross-cut figures presented in Fig. 2 one can note that there is a clear propagation path through the outer and

TABLE 1. Comparison between ring antenna and reference antenna at antenna locations 1 and 2.

	Antenna location 1		Antenna location 2	
	Path loss at 4 GHz [dB] Ring / reference antenna	Level of the impulse response's main peak [dB]	Path loss at 4 GHz [dB]	Level of the impulse response's main peak [dB]
Left	75 / 74	-72 / -75	85 / 80	-85 / -84
Middle	58 / 40	-65 / -45	58 / 52	-68 / -60
Right	95 / 85	-80 / -95	60 / 82	-62 / -88

inner fat tissues between the capsule's location "right" and the on-body antenna location 2. The path goes between the abdominal muscle elements and via the inner fat between the intestine elements. As explained in [18], [20], [33], [34], fat is a good propagation medium inside the human body due to its dielectric properties. Propagation paths through the fat layer enables that even deeper capsule locations in the small intestine can be achieved with reasonable losses. Due to this propagation path through the fat layers, the path loss difference between the capsule locations "middle" and "right" is minor. Also, the power flows presented in Fig. 12 a show that capsule locations "middle" and "right" are reached within −70 dB range. Instead, the capsule location left is out of this frequency range.

In time domain, the difference between the impulse responses can be seen in the shapes and timings of the main peaks. Width of the main peak for capsule location "middle" and the on-body antenna is remarkably larger than that for the capsule location "right" and the on-body antenna. This is due to the fact that between the capsule location "middle" and on-body antenna, there is more propagation paths through the fat layer available. The differences in the levels of the main peaks are minor, maximum 3 dB. Level of the impulse response's main peak in the capsule location "left" is −84 dB.

The channel behavior with the reference antenna is somewhat similar at the capsule locations "middle" and "left". Instead, the capsule location "right" completely different: path loss is at the same level as in the capsule location "left". This is interesting result, since in the case of Ring antenna, the channel for the capsule location "right" was at the same level as the capsule location "middle". When we study power flows presented in Fig 12b, we can see that at the selected horizontal cross-cut level, the power flow reaches the small intestine except at the capsule location "right". That area is out of the dB range of interest. Thus, the channel with the reference antenna is weak in that capsule location. Assumedly even small shift of the capsule in the small intestine could improve the channel significantly. Table 1 summarizes the comparison between the Ring antenna and reference antenna in the antenna locations 1 and 2.

C. ANTENNA LOCATION 3

Finally, the channel characteristics between the capsule and the on-body antenna are evaluated with the Ring antenna on-body antenna location 3 and capsule location "right".

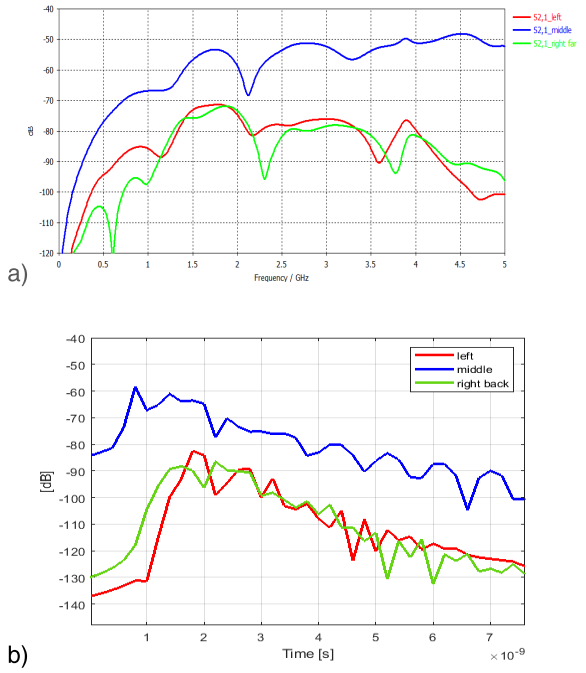

FIGURE 18. a) Frequency and b) time domain channel characteristics at the on-body antenna location 2 obtained with the reference antenna.

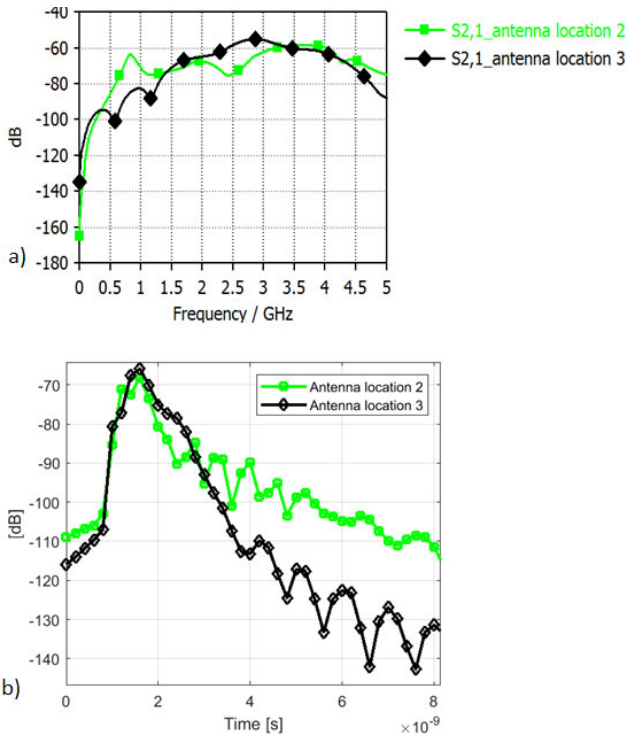

FIGURE 19. a) Frequency and b) time domain channel characteristics at the on-body antenna location 2 and 3 obtained with the Ring antenna.

The frequency and time domain channel characteristics are presented in Fig. 19a–b. The main motivation for this evaluation is to find if one can get better view on the capsule location ''right'' by transferring the on-body antenna 4 cm towards right on the abdomen area. Thus, the results are compared only with the frequency and time domain channel results obtained with on-body antenna location 2 in the capsule location ''right''. It was interesting to note that the path loss difference between the on-body antenna location 1 and 2 in the capsule location ''right'' is very minor in the frequency range of interest; merely 2 dB at 3.75 GHz. Also, the impulse responses for the first 2 ns are almost same. The main difference is on the side peaks, i.e., in the different alternative propagation paths.

Same propagation path through the fat layer is used as the signal propagates from the capsule towards the on-body antenna location 2. Although the on-body antenna in the location 2 is slightly further from the capsule than in the location 3, the difference is minor when taking into account the cavity width. Thus, the path loss difference is somewhat same in the link between the capsule on the location ''right'' and the on-body antenna on the locations 2 and 3.

D. COMPARISON WITH DIFFERENT VOXEL MODELS

This section compares frequency and time domain channel characteristics obtained with Laura, Donna, Gustav, and Hugo voxel models, whose cross-cuts were presented in Section II in Figs. 2a–d, respectively. The first aim is to find the channel characteristics between the capsule and the Ring on-body antenna in the on-body antenna location 1, which is considered among the most suitable on-body antenna location for the capsule communications. Figs. 2a–d presents also capsule locations used in this study case. The second aim is to evaluate channel characteristics on the location where the thicknesses of the muscle layer and fat layer have impact on the capsule link: i.e., antenna location 2 and capsule location ''front right''. As it can be seen for Fig. 2, for Donna there is no abdominal muscle layer at the right part of the abdomen at this cross-cut level. Thus, we select the antenna location 4 and capsule location ''left'' for Donna for these evaluations. Similarly, we select antenna location 4 to Hugo, since Hugo does not have small intestine at the right part of the abdomen at this cross-cut level. The on-body antenna and capsule locations are marked in Figs. 20a–d.

One can note from Figs. 2 and 20 that with different voxel models, the thicknesses of the tissues between the capsule and the on-body antenna may vary significantly. Even in the antenna location 1, there are clear differences. Besides, the size of the navel varies a lot, which can have strong impact on the channel in this antenna locations. For instance, Donna has a very deep navel, Hugo a very wide navel and Laura a very flat navel. As stated in Section II, there is no small intestine for Gustav model at navel level and thus, this case is evaluated slightly above the navel.

E. CHANNEL CHARACTERISTICS AT ANTENNA LOCATION 1

Frequency and time domain channel characteristics for different voxels are presented in Figs. 21a–b. It is found that

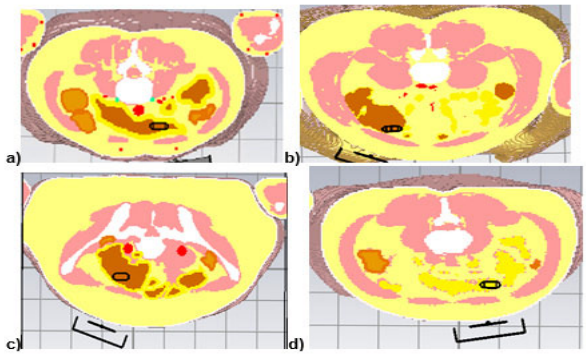

FIGURE 20. Cross-sections of the voxel models a) Laura, b) Donna, c) Gustav, d) Hugo.

path loss between the capsule and the on-body antenna link with different voxel models may vary significantly along the simulated frequency range. For instance, at 2.25 GHz, the path loss with Gustav voxel model is 25 dB smaller than that with Hugo voxel model. However, within the frequency range of interest, i.e., antenna's operational frequency range 3.75 – 4.25 GHz, the path loss differences are minor, maximum 4 dB between Gustav, Hugo, Donna. The path loss with Laura voxel model differs at maximum 4 dB from the path losses of the other voxels within 3.74 – 4 GHz, but at 4.1 – 4.25 GHz the difference is almost 10 dB. This is a surprising result, since Laura voxel is one of the leanest voxel models with less tissues between the capsule and the on-body antenna. Hence, the loss for the signal transmitted from to the capsule towards the on-body antenna, was assumed to be among the smallest.

In time domain channel characteristics, presented in Fig. 21b, difference between the main peaks level obtained with different voxel model, is minor: only maximum 2.5 dB. Surprisingly, the highest peaks are obtained with the overweight models Donna and Hugo. There are clear differences in the shapes of the main peaks: Donna and Hugo have the widest peaks and Laura and Gustav have the narrower peaks. Besides, there are clear differences in the levels and shapes of the side peaks.

There are some possible reasons for these path loss comparison results. First is the voxel models' different pixelization, which can have impact on the actual antenna-body distance as explained in [19]. Even small differences in the antenna-body distances cause clear difference in the antenna matching [27], and, also in the channel characteristics [35]. Besides, differences in the pixel size cause differences in the skin surface below the antenna, which can have clear impact on the antenna matching as well as on the channel characteristics, as explained in [36]. Antenna matching can be studied in Fig. 22c, which presents the antenna reflection coefficients S22 with different voxel models at the antenna location 1. It is found that S22 may vary significantly with different voxel models. Interestingly, S22 with Laura is not the weakest one and hence, the antenna reflection coefficients

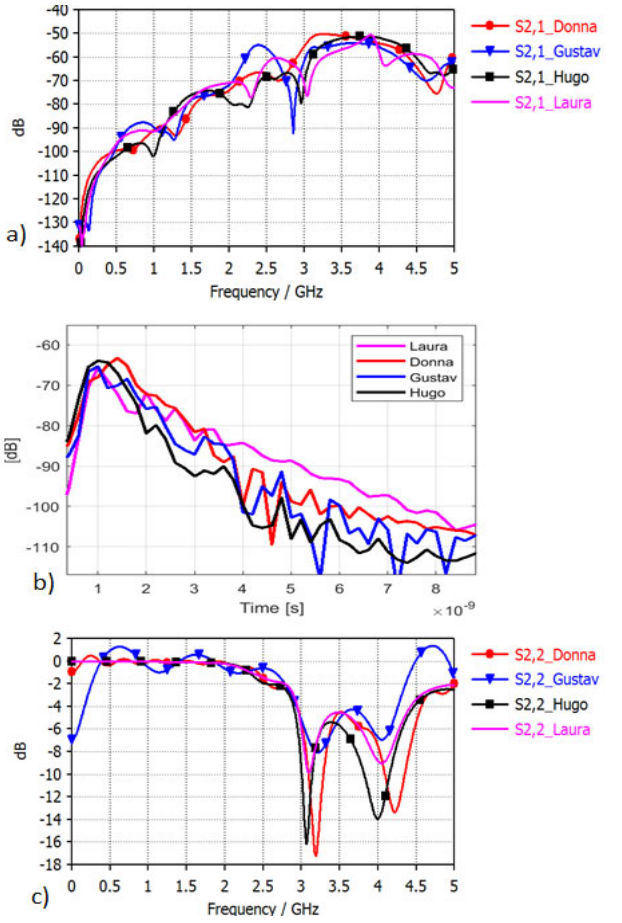

FIGURE 21. a) Frequency and b) time domain channel characteristics and c) on-body antenna reflection coefficients (Ring) with different voxel models at the antenna location 1.

do not explain the reason for larger path loss with Laura-voxel at 4 – 4.25 GHz. As discussed earlier, the pixel size causes differences in the antenna matching. However, the main reason for the differences between the S22s obtained with different voxel models is the differences between the thicknesses of the tissues between. Reference [28] present reflection coefficients simulated with layer models having different thicknesses for the fat and muscle layers. In that study case, difference between the layer models resembling the ''lean'' and ''overweight'' cases is minor. However, as shown in the measurement -based studies presented in [34] with the reference on-body antenna prototype, the measured antenna reflection coefficient may vary clearly between different volunteers having different body constitutions.

The physical structure of the voxel model's abdomen area may have impact on the reflection coefficient. Especially in this antenna location, where the antenna is located on the navel, the dimensions of the navel are assumed to have a clear impact. The larger the navel, the more air below the antenna, which improves antenna reflection coefficients. As discussed earlier, Hugo's and Donna's navels are larger than Laura's. In Gustav's case, the antenna is located slightly upwards from

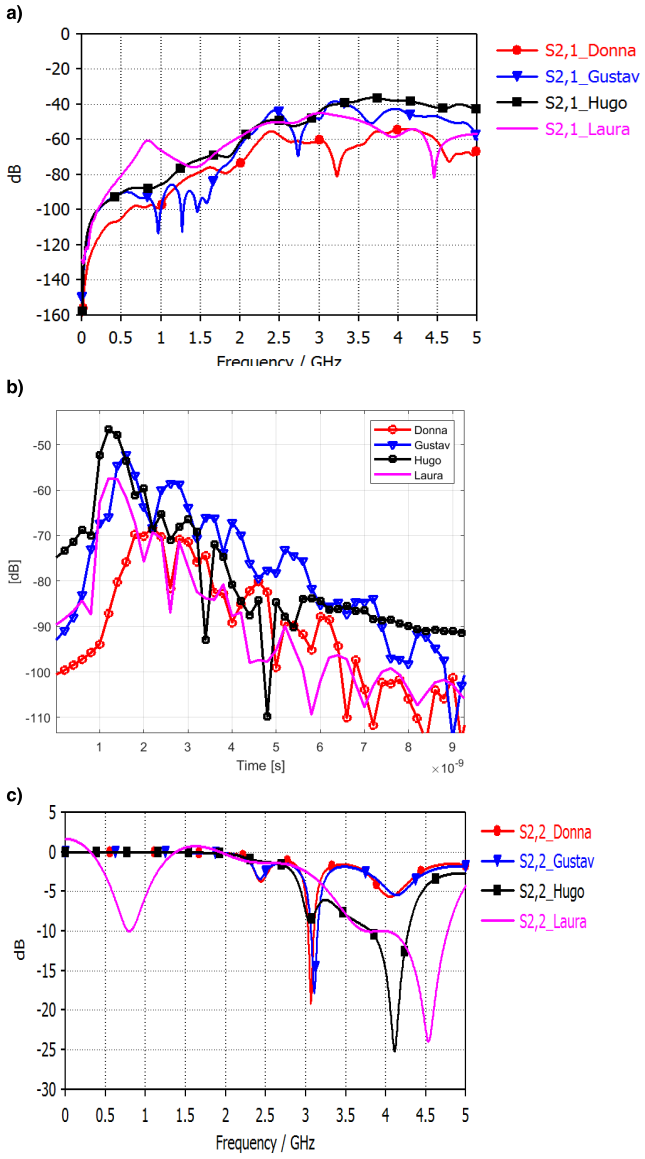

FIGURE 22. a) Frequency and b) time domain channel characteristics, and c) antenna reflection coefficients at the on-body antenna location 2 or 4.

the navel and hence there is no additional air gap due to the navel. As discussed in [7], the additional air gap due to the navel below the antenna improves the antenna performance and thus, it is understandably that the antenna reflection coefficient with Gustav (on that antenna location) is weaker than the others. On the other hand, it is logical that the antenna reflection coefficient with Hugo model, which has the widest navel, is better than the others.

Hugo's and Donna's navels are also noted to be quite deep, which enables the signal transmitted from the capsule to travel partly through the air. This provides explanation why the channel between the capsule and the on-body antenna is strong even with these overweight voxel models whose skin-small intestine distance is remarkably larger than those with the leaner voxel models.

As one can note from Figs. 2a–c, that except of the navel area, the abdominal area at these cross-cuts levels are very similar to Laura and Gustav. Thus, the channel results between Laura and Gustav provide information how much navel has impact on the results. We can note from Fig. 19b that the level of the impulse response's side peak obtained with Laura are clearly higher than those obtained with Gustav model, except at the time instant 1.7 ns. The reason for higher side peaks is due to signals' possibility to travel partly through the air in the navel area. Since there is no navel in the Gustav model at this cross-cut level, the signals travel until the on-body antenna only through the tissues which naturally yields higher propagation losses. The reason for the higher side peak with Gustav-voxel at 1.7 ns is unknown and is left for future's study.

F. CHANNEL CHARACTERISTICS AT ANTENNA LOCATION 2

Next, we present the channel characteristics between the capsule and the on-body antenna as the on-body antenna is located on the side (antenna location 2 or 4). The frequency and time domain channel characteristics for all the voxels are presented in Figs. 22a–b. The reflection coefficients are presented in Fig. 22c. As one can note, in this case we see clearer differences in the channel obtained with different voxels. The path loss difference is surprisingly large between the best and worst cases: even 20 dB within frequency range of interest. Interestingly, the path loss with Hugo model has the lowest path loss, only 40 dB within the frequency range of interest, although the muscle and outer fat layers are relatively thick in Hugo model. Also, Gustav's path loss is relatively small: 45 dB. The strongest path losses are with Donna and Laura: 60 dB. In time domain, the differences between the main peaks are even more remarkable: the main peak levels obtained with Hugo, Gustav, Donna and Laura are at −46 dB, −52 dB, −58 dB, and −70 dB, respectively. Donna's weak channel is understandable due to the thick fat layers, whereas Laura's weak channel and Hugo's strong channel needs more detailed evaluations. Firstly, the antenna matchings are studied in Fig. 22c, where the reflection coefficients for each model are presented. As it is noted, S22 can be significantly different with different voxel models. The antenna matching is the best with Hugo voxel: S22's notch is at 4 GHz whereas in Donna's and Gustav's case, notch is shifted to 3 GHz and in Laura's case shifted to 4.5 GHz. Antenna matching explains the channel behavior partly.

Next the tissues between the capsule and the on-body antenna in the voxel models' cross-cuts are studied more in details from Fig.18. In Laura's case, there is relatively thick and wide muscle between the capsule and the on-body antenna. This is one reason for high path loss in Laura's case, since the propagation loss in the muscle layers is high [31]. However, fat on the both sides of the muscle layers provide propagation path with minor losses [20], [33], [34]. In the case of Donna, there is also muscle layer between the capsule and the on-body antenna, but the most significant difference comes from the thickness of the outer fat layer: it is three time

TABLE 2. Path loss and IR main peak level comparison between different voxel models at antenna locations 1 and 2.

	Antenna location 1		Antenna location 2	
	Path loss at 4 GHz [dB]	Level of the impulse response's main peak [dB]	Path loss at 4 GHz [dB]	Level of the impulse response's main peak [dB]
Laura	57	-67	60	-58
Donna	54	-64	56	-70
Gustav	55	-67	42	-52
Hugo	52	-63	40	-47

wider than with Laura voxel. In Donna's case, on the side of the abdominal muscle, there is also a fat tissue providing propagation path for the signal transmitted from the capsule.

In Gustav's case, the muscle layer between the capsule and the on-body antenna is thicker than with Laura and Donna. Gustav's outer fat layer is only slightly thicker than Laura's in that area. However, the main difference between the Laura and Gustav models is the fat propagation path from the capsule towards the on-body antenna. In the case of Gustav model, this ''fat path'' is available directly after the signal transmitted from the capsule passes the small intestine. Instead in the case of Laura, the muscle layer is like a barrier between the capsule and the on-body antenna, and hence the fat path is less reachable. Thus, the path loss is clearly larger with Laura than with Gustav models.

Hugo's case was studied more in details to find reason for surprisingly strong channel. Detailed study revealed that Hugo's skin on the abdomen area is like reticulated: full of holes. Due to these holes, the signal can propagate directly from the fat tissue to the on-body antenna without passing the skin layer. The picture of Hugo's skin layer is plotted separately in Fig. 23a. As a comparison, Laura's skin layer, which is complete and smooth, is plotted in Fig. 23b. As conclusions, Hugo's reticulated skin is reason for lowest path loss in addition to the best antenna matching. After finding the skin problem in Hugo's abdominal area, the authors however decided to include the results with Hugo on the paper, since Hugo is a commonly used voxel model in the literature also in the abdominal implant channel modeling studies. The partial lack of the skin change antenna matching as well as diminish the propagation loss, which should be taken into the account.

Finally, the values for path loss at 4 GHz and the levels of the impulse response's main peaks obtained with different voxel models are summarized in Table 2. The table covers values for both on-body antennas and antenna location options. Table 2 elucidates the main findings of the channel evaluation results from the previous sections: the size and body constitution of the voxel model has clearly more impact in the antenna location 2 than antenna location 1. This is due to the fact, that antenna location 1 is a special case as the navel provides additional air below the antenna and there is less issues to propagate through. Thus, it is considered one of the best on-body antenna locations for the abdominal implant communication system.

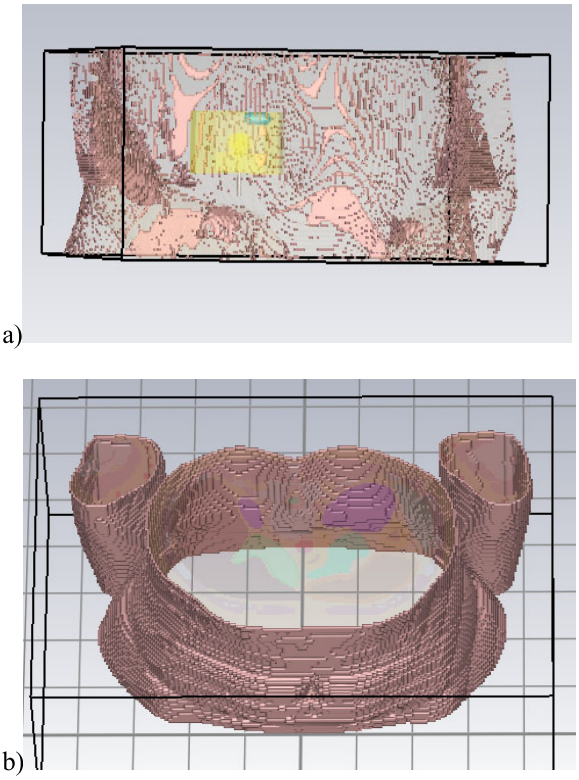

FIGURE 23. Skin layer plotted separately for a) Hugo and b) Laura voxels.

V. IMPACT OF THE CAPSULE'S ROTATION

The impact of the capsule's rotation is evaluated with Laura-voxel model using the Ring antenna. We evaluated the rotation angles 0°, 45° and 90°, which are presented in vertical cross-sections in Figs. 24a–c. Similar comparison has been made in [19] with the reference on-body antenna. The differences of the results are discussed here as well.

First the voxel model results are evaluated in frequency and time domains, as presented in Figs. 25a–b, respectively. As one can note, there are clear differences in path loss values within the frequency range of interest. The path loss is lowest with the capsule rotation angle 0°, whereas the path loss is highest as the capsule is rotated 90°. The path difference between these cases is at maximum 7 dB within the frequency range of interest. The path loss with the rotation angle 45° is approximately between the path losses obtained with the rotation angle cases 0° and 90° degrees. Outside the frequency range of the interest, the path loss difference is remarkably higher and also the path loss order changes at certain frequencies.

In time domain, the difference between the main peaks of the CIRs obtained with the rotation angles 0° and 90° is 7 dB. Interestingly, the highest peak of the CIR for rotation angle 45° arrives 0.5 ns later than for the rotation angle cases 0° and 90°. Besides, there are clear differences in the shape of the CIRs for the first 2 ns. The reason for this is that with rotation angle case 45°, the optimal propagation paths are assumably slightly different than for the rotation angle cases 0° and 90°.

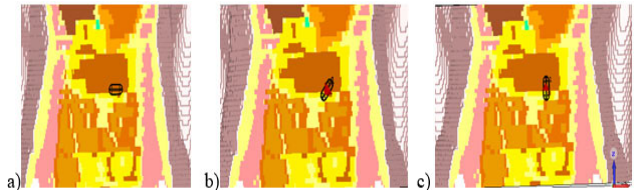

FIGURE 24. Capsule's rotation angle a) 0°, b) 45°, and c) 90°.

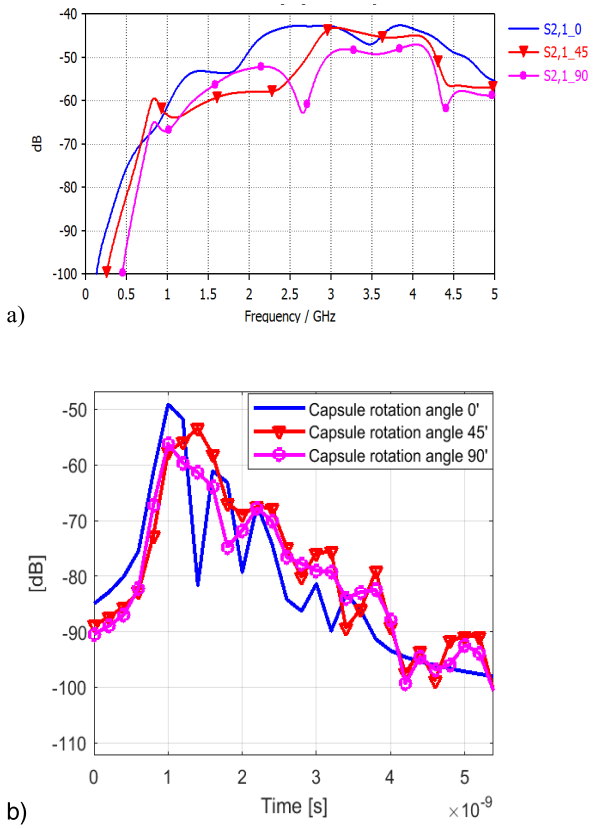

FIGURE 25. Impact of the rotation with a) frequency and b) time domain channel characteristics using Laura-voxel model and Ring antenna at antenna location 2.

TABLE 3. Path loss comparison between the Ring and reference antennas with different rotation angles.

Frequency Path loss (dB)	3.75 GHz Rotation angles 0°, 45°, 90°	4 GHz Rotation angles 0°, 45°, 90°	4.25 GHz Rotation angles 0°, 45°, 90°
Ring antenna	45, 42, 48	44, 46, 48	45, 50, 52
Ref. antenna	42, 45, 50	43, 43, 58	48, 48, 52
Difference	-3, 3, 2	-1, -3, 10	3, -2, 0

Next we compare these rotation angle results to the rotation angle study we presented in [19] with the reference on-body antenna introduced in [26]. The results are repeated Fig. 26a–b for the clarity to ease the comparison between these two cases. As one can see, similar tendency can be

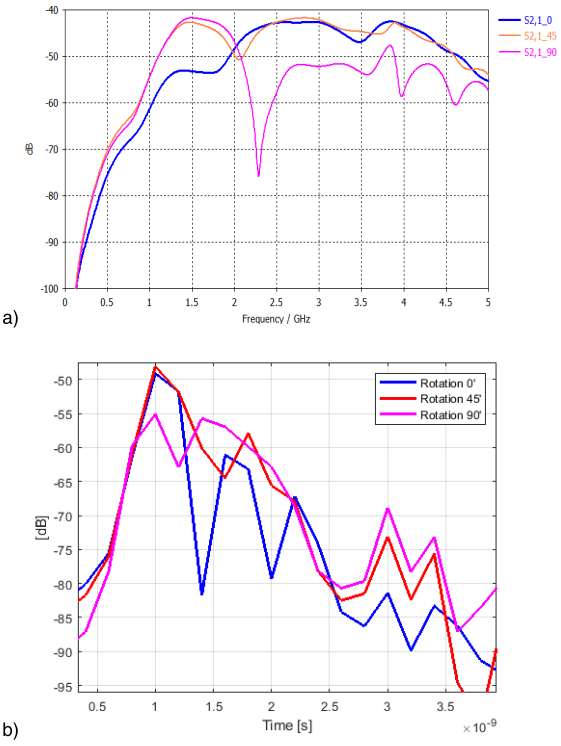

FIGURE 26. Impact of the rotation in a) frequency and b) time domain channel characteristics with Laura-voxel model and reference antenna at antenna location 2.

found in the case of the other antenna: the lowest and highest path losses are obtained in the cases of rotation angles 0° and 90°. Instead, the difference between the rotation angles cases 0° and 45° is surprisingly small with the reference antenna. The main difference is in the side peaks of the impulse responses.

There are several possible reasons for differences in the impact of the capsule rotation. For instance, the cavity and its size may have strong impact. Cavity affects clearly on the radiation patterns of the antennas as presented in [27], [28]. Differences in the radiation patterns may cause that the propagation paths with low attenuation coincide with low antenna gain direction for one of the antennas while the other antenna has higher antenna gain in that direction. The larger is the cavity, the wider is the area in which different propagation paths from the capsule endoscope are summed up in the on-body receiving antenna.

Finally, we compare the path losses obtained with these two antennas with the capsule rotation angles 0°, 45°, and 90°. To avoid excessive number of the figures, path loss values with different rotation angles at frequency points 3.75 GHz, 4 GHz, and 4.25 GHz are presenetd in Table 3. Also, the path loss difference respect to the Ring antenna's values are included in the table. The positive path loss values mean that the path loss with Ring antenna is smaller, whereas the negative value mean that the path loss with Ring antenna is larger. One can note that path loss difference between the antennas with rotation angles 0° and 45° is relatively minor,

whereas there is a clear difference in path loss values with the rotation angle 90°. With linearly polarized antennas, the rotation angle 90° is obviously the most challenging position. and then the on-body antenna gain towards the capsule plays crucial role. The power flows from these on-body antennas are presented in [7].

VI. SUMMARY AND CONCLUSION

This paper presented a study on the radio channel characteristics between the capsule endoscope and two directive on-body antennas in different parts of the small intestine with different on-body antenna locations. The study was conducted using finite integration technique based electromagnetic simulation software CST and four of its anatomical voxel models. Channel characteristics were evaluated both in frequency and time domains. Furthermore, propagation within the tissues was studied with 2D power flow representations in the cross-cuts of the voxel models. A capsule endoscope model was set inside different areas of the small intestine of the voxel model and channel characteristics were evaluated with different on-body antenna locations. The impact of capsule's different rotation angles on the channel characteristics were also evaluated.

It is found that the radio channel characteristics varied remarkably depending on the capsule location in the small intestine as well as location of the on-body antennas. The difference in the channel strengths obtained with two on-body antennas varied between 0 – 20 dB depending on the on-body antenna location and the capsule locations. The difference is due to the different antenna radiation patterns of the on-body antennas.

Power flow studies show that the Ring antenna has weaker direct beam from the antenna towards the body than the reference antenna due to the Ring antenna's smaller cavity size. Instead, power flow on the sides of the voxel is stronger which in some cases enabled stronger propagation paths through the outer and inner fat towards the deepest parts of the small intestine. For instance, with the Ring antenna, the impulse response's main peak was above −85 dB in all the studied cases. Instead with the reference antenna, the channel strength was strong as the physical distance between the capsule and the on-body antenna was small, but the main peaks of the impulse responses were even below −90 dB as the capsule was located further from the on-body antenna. Hence, for the practical solutions, on-body antennas having similar characteristics as Ring antenna would also suit well for capsule communications.

This result is considered positive since Ring antenna's cavity is clearly smaller and lighter than that of the reference antenna. Hence, even the on-body antennas with lighter cavity sizes can also be suitable for implant communications if the antenna locations are determined in an appropriate way to maximize the power flow though the inner and outer fat layer taking into the account on-body antenna's radiation characteristics in the presence of the human body. In other words, since the propagation loss in the muscles is so high, the on-body antennas having strong beam towards the body should be located between the abdominal muscles so that the strongest lobe is directed towards visceral fat layers. In the case of antennas with minor direct beam towards the body, the antennas could be set above the muscle layers so that lobes heading to sides would reach easily the visceral fat layer. One of our future's work item is to study the impact of the cavity in more details.

In this study, we used a simple dipole antenna on the capsule. The path loss due to capsule's rotation could be diminished with circular-polarized antennas, either on the body or inside the capsule. Our future target is to evaluate channel characteristics with circularly-polarized antennas. Furthermore, the impact of the rotation angle will be studied more in details. Besides, we aim to make evaluations with more realistic capsule structures. Moreover, one of the plans is to evaluate bit-error-rate (BER) performance with impulse radio (IR) UWB transceiver simulator using the channel responses simulated in different part of the small intestine. Finally, our aim is to conduct measurements with prototypes and different phantoms.

ACKNOWLEDGMENT

Dr. M. Sonkki is acknowledged for his participation on the on-body antenna design.

REFERENCES

[1] G. Ciuti, A. Menciassi, and P. Dario, "Capsule endoscopy: From current achievements to open challenges," *IEEE Rev. Biomed. Eng.*, vol. 4, pp. 59–72, 2011.

[2] H. Neumann, L. C. Fry, A. Nägel, and M. F. Neurath, "Wireless capsule endoscopy of the small intestine: A review with future directions," *Current Opinion Gastroenterol.*, vol. 30, no. 5, pp. 463–471, Sep. 2014.

[3] D. R. Cave, S. Hakimian, and K. Patel, "Current controversies concerning capsule endoscopy," *Digestive Diseases Sci.*, vol. 64, no. 11, pp. 3040–3047, Nov. 2019.

[4] O. Bchir, M. M. Ben Ismail, and N. AlZahrani, "Multiple bleeding detection in wireless capsule endoscopy," *Signal, Image Video Process.*, vol. 13, no. 1, pp. 121–126, Feb. 2019.

[5] R. Chavez-Santiago, J. Wang, and I. Balasingham, "The ultra wideband capsule endoscope," in *Proc. IEEE Int. Conf. Ultra-Wideband (ICUWB)*, Sep. 2013, pp. 72–78.

[6] S. Stoa, R. Chavez-Santiago, and I. Balasingham, "An ultra wideband communication channel model for capsule endoscopy," in *Proc. 3rd Int. Symp. Appl. Sci. Biomed. Commun. Technol. (ISABEL)*, Nov. 2010, pp. 1–5.

[7] *IEEE Standard for Local and Metropolitan Area Networks_Part 15.6: Wireless Body Area Networks*, IEEE Standard 802.15.6-2012, Feb. 2012, pp. 1–271.

[8] X. Fang, M. Ramzan, Q. Zhang, S. Perez-Simbor, Q. Wang, N. Neumann, C. Garcia-Pardo, N. Cardona, and D. Plettemeier, "Experimental in-body to on-body and in-body to in-body path loss models of planar elliptical ring implanted antenna in the ultra-wide band," in *Proc. 13th Int. Symp. Med. Inf. Commun. Technol. (ISMICT)*, May 2019, pp. 1–5.

[9] A. F. Demir, Q. H. Abbasi, Z. E. Ankarali, A. Alomainy, K. Qaraqe, E. Serpedin, and H. Arslan, "Anatomical region-specific *in vivo* wireless communication channel characterization," *IEEE J. Biomed. Health Inform.*, vol. 21, no. 5, pp. 1254–1262, Sep. 2017.

[10] J.-C. Brumm, H. Strohm, and G. Bauch, "A stochastic channel model for ultra wideband in-body communication," in *Proc. 41st Annu. Int. Conf. IEEE Eng. Med. Biol. Soc. (EMBC)*, Jul. 2019, pp. 4032–4035.

[11] J. Li, Z. Nie, Y. Liu, L. Wang, and Y. Hao, "Characterization of in-body radio channels for wireless implants," *IEEE Sensors J.*, vol. 17, no. 5, pp. 1528–1537, Mar. 2017.

[12] P. Turalchuk, I. Munina, V. Pleskachev, V. Kirillov, O. Vendik, and I. Vendik, "In-body and on-body wave propagation: Modeling and measurements," in *Proc. Int. Workshop Antenna Technol., Small Antennas, Innov. Struct., Appl. (iWAT)*, Mar. 2017, pp. 154–157.

[13] A. Alomainy and Y. Hao, "Modeling and characterization of biotelemetric radio channel from ingested implants considering organ contents," *IEEE Trans. Antennas Propag.*, vol. 57, no. 4, pp. 999–1005, Apr. 2009.

[14] Y. El-Saboni, G. A. Conway, S. L. Cotton, and W. G. Scanlon, "Radiowave propagation characteristics of the intra-body channel at 2.38 GHz," in *Proc. IEEE 14th Int. Conf. Wearable Implant. Body Sensor Netw. (BSN)*, May 2017, pp. 149–152.

[15] C. Garcia-Pardo, A. Fornes-Leal, N. Cardona, R. Chavez-Santiago, J. Bergsland, I. Balasingham, S. Brovoll, O. Aardal, S.-E. Hamran, and R. Palomar, "Experimental ultra wideband path loss models for implant communications," in *Proc. IEEE 27th Annu. Int. Symp. Pers., Indoor, Mobile Radio Commun. (PIMRC)*, Sep. 2016, pp. 1–6.

[16] M. Särestöniemi, C. Pomalaza-Raez, C. Kissi, M. Hämäläinen, and J. Iinatti, "Impact of the antenna-body distance on the WBAN channel characteristics," in *Proc. 13th Int. Symp. Med. Inf. Commun. Technol. (ISMICT)*, May 2019, pp. 1–6.

[17] N. Asan, E. Hassan, J. Shah, D. Noreland, T. Blokhuis, E. Wadbro, M. Berggren, T. Voigt, and R. Augustine, "Characterization of the fat channel for intra-body communication at R-Band frequencies," *Sensors*, vol. 18, no. 9, p. 2752, 2018.

[18] M. Särestöniemi, C. Pomalaza-Raez, M. Berg, C. Kissi, M. Hämäläinen, and J. Iinatti, "In-body power distribution for abdominal monitoring and implant communications systems," in *Proc. 16th Int. Symp. Wireless Commun. Syst. (ISWCS)*, Aug. 2019, pp. 457–462.

[19] M. Särestöniemi, C. Pomalaza-Raez, M. Berg, C. Kissi, M. Hämäläinen, and J. Iinatti, "UWB-WBAN Radio Channel Characteristics between the Endoscope Capsule and On-body Antenna," in *Proc. Bodynets*, Oct. 2019, pp. 1–17.

[20] M. Särestöniemi, C. Pomalaza-Raez, T. Kumpuniemi, C. Kissi, M. Hämäläinen, and J. Iinatti, "Fat in the abdomen as a propagation medium in WBAN applications," in *Proc. Bodynets*, Oct. 2019, pp. 18–27.

[21] Y. Morimoto, D. Anzai, and J. Wang, "Design of ultra wide-band low-band implant antennas for capsule endoscope application," in *Proc. 7th Int. Symp. Med. Inf. Commun. Technol. (ISMICT)*, Mar. 2013, pp. 61–65.

[22] G. A. Conway and W. G. Scanlon, "Wearable antennas for medical monitoring systems," in *Proc. Int. Workshop Antenna Technol. (iWAT)*, Mar. 2015, pp. 19–21.

[23] S. H. Lee, J. Lee, Y. J. Yoon, S. Park, C. Cheon, K. Kim, and S. Nam, "A wideband spiral antenna for ingestible capsule endoscope systems: Experimental results in a human phantom and a pig," *IEEE Trans. Biomed. Eng.*, vol. 58, no. 6, pp. 1734–1741, Jun. 2011.

[24] W. Lei and Y.-X. Guo, "Design of a dual-polarized wideband conformal loop antenna for capsule endoscopy systems," *IEEE Trans. Antennas Propag.*, vol. 66, no. 11, pp. 5706–5715, Nov. 2018.

[25] A. A. Balabel, H. A. Malhat, and S. H. Zainud-Deen, "Circularly-polarized 4-arm curl antenna for wireless capsule endoscopy," in *Proc. 35th Nat. Radio Sci. Conf. (NRSC)*, Mar. 2018, pp. 22–29.

[26] C. Kissi, M. Särestöniemi, C. Pomalaza-Raez, M. Sonkki, and M. N. Srifi, "Low-UWB directive antenna for wireless capsule endoscopy localization," in *Proc. BodyNets*, 2018, pp. 431–442.

[27] C. Kissi, M. Särestöniemi, T. Kumpuniemi, M. Sonkki, S. Myllymaki, M. N. Srifi, and C. Pomalaza-Raez, "Low-UWB receiving antenna for WCE localization," in *Proc. 13th Int. Symp. Med. Inf. Commun. Technol. (ISMICT)*, May 2019, pp. 1–6.

[28] C. Kissi, M. Särestöniemi, T. Kumpuniemi, J.-P. Mäkelä, M. Sonkki, S. Myllymäki, M. N. Srifi, H. Jantunen, and C. P-. Raez, "Receiving UWB antenna for capsule endoscope communications," in *Proc. PIERS*, Mar. 2020, p. 20.

[29] *CST Microwave Studio*. Accessed: Jan. 11, 2011. [Online]. Available: http://www.cst.com

[30] S. J. Orfanidis, "Electromagnetic waves and antennas," ECE Dept., Rutgers Univ., Piscataway, NJ, USA, Tech. Rep., 2002. Accessed: Oct. 30, 2018. [Online]. Available: http://www.ece.rutgers.edu/~orfanidi/ewa/

[31] *It'Is Foundation, Dielectric Properties For the Materials*. Accessed: Jul. 31, 2017. [Online]. Available: https://www.itis.ethz.ch/virtual-population/tissue-properties/database

[32] M. Särestöniemi, C. Pomalaza-Ráez, Z. Bi, T. Kumpuniemi, C. Kissi, M. Sonkki, M. Hämäläinen, and J. Iinatti, "Comprehensive study on the impact of sternotomy wires on UWB WBAN channel characteristics on the human chest area," *IEEE Access*, vol. 7, pp. 74670–74682, 2019, doi: 10.1109/ACCESS.2019.2920067.

[33] N. B. Asan, D. Noreland, E. Hassan, S. R. M. Shah, A. Rydberg, T. J. Blokhuis, P.-O. Carlsson, T. Voigt, and R. Augustine, "Intra-body microwave communication through adipose tissue," *Healthcare Technol. Lett.*, vol. 4, no. 4, pp. 115–121, Aug. 2017.

[34] N. B. Asan, E. Hassan, J. Velander, M. Shah, S. Redzwan, M. Shah, D. Noreland, T. J. Blokhuis, E. Wadbro, M. Berggren, T. Voigt, and R. Augustine, "Characterization of the fat channel for intra-body communication at R-band frequencies," *Sensors*, vol. 18, no. 9, p. 2752, 2018.

[35] M. Särestöniemi, C. Kissi, C. Pomalaza-Raez, T. Kumpuniemi, M. Sonkki, S. Myllymäki, M. Hämäläinen, and J. Iinatti, "Measurement and simulation based study on UWB channel characteristics on the abdomen area," in *Proc. 13th Int. Symp. Med. Inf. Commun. Technol. (ISMICT)*, May 2019, pp. 1–6.

MARIELLA SÄRESTÖNIEMI received the M.Sc. and Lic.Tech. degrees from the University of Oulu, Finland, in 2003 and 2005, respectively, where she is currently pursuing the Ph.D. degree with the Centre for Wireless Communications. Her research interests are medical ICT, wireless body area networks, in-body and on-body communications, and simulation-based channel modeling and measurements.

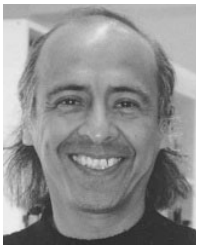

CARLOS POMALAZA-RÁEZ (Senior Member, IEEE) received the B.S.M.E. and B.S.E.E. degrees from the Universidad Nacional de Ingeniería, Lima, Peru, in 1974, and the M.S. and Ph.D. degrees in electrical engineering from Purdue University, West Lafayette, IN, USA, in 1977 and 1980, respectively. From 2003 to 2004, under the auspices of a Nokia-Fulbright Scholar Award, he was a Visiting Professor with the Centre of Wireless Communications, University of Oulu, Oulu, Finland. He is currently a Professor of electrical engineering with Purdue University at Fort Wayne, Fort Wayne, IN, USA. He has been a Faculty Member with the University of Limerick, Limerick, Ireland, and with Clarkson University, Potsdam, NY, USA. He has also been a member of the Technical Staff with the Jet Propulsion Laboratory, California Institute of Technology, Pasadena, CA, USA. His research interests include wireless communications networks and signal processing applications.

CHAÏMAÂ KISSI received the degree in engineering from the National School of Applied Sciences (ENSA), Ibn Tofail University, Kenitra, Morocco, in 2015, where she is currently pursuing the Ph.D. degree with the Electronics and Telecommunication Systems Research Group. Her research focus is antenna design for medical applications.

MARKUS BERG received the M.Sc. (Tech.) and D.Sc. degrees in electrical engineering from the University of Oulu, Oulu, Finland, in 2005 and 2011, respectively.

From 2005 to 2015, he was a Research Scientist and the Project Manager with the Centre for Wireless Communications, University of Oulu. In 2015, he was a Design Engineer with Elektrobit, Oulu, and Bittium Corporation, Oulu. He is currently a co-founder of ExcellAnt Ltd., where he works as a part-time Senior Antenna Advisor. He is also an Adjunct Professor with the Faculty of Information Technology and Electrical Engineering, University of Oulu. His current research interests include antennas and propagation for wireless communication, THz integrated antennas, wearable antennas and antennas for small devices, and GNSS reflectometry. He has authored or coauthored more than 70 international journal and conference papers.

MATTI HÄMÄLÄINEN (Senior Member, IEEE) received the M.Sc., Lic.Tech., and Dr.Sc. degrees from the University of Oulu, Finland, in 1994, 2002, and 2006, respectively. He is currently an Adjunct Professor and a University Researcher with the Centre for Wireless Communications, University of Oulu, and an IAS Visiting Professor with Yokohama National University, Japan. He has more than 150 scientific publications. He is also co-editor of one book, and coauthor of one book and two book chapters. His research interests are in ultra wideband systems, radio channel modeling, wireless body area networks, and medical ICT. He has served as a Technical Program Committee Member for numerous IEEE conferences. He is also a member of the European Telecommunications Standard Institute (ETSI) Smart Body Area Network (SmartBAN) Group. He has also served as a reviewer for the IEEE and IET journals.

JARI IINATTI (Senior Member, IEEE) received the M.Sc., Lic.Tech., and Dr.Tech. degrees in electrical engineering from the University of Oulu, Oulu, Finland, in 1989, 1993, and 1997, respectively. From 1989 to 1997, he was a Research Scientist with the Telecommunication Laboratory, University of Oulu, where he was an Acting Professor of digital transmission techniques, a Senior Research Scientist, the Project Manager, and the Research Director with the Centre for Wireless Communications (CWC), from 1997 to 2002. Since 2002, he has been a Professor of telecommunication theory, where he is currently the Head of the CWC–Networks and Systems, as well as the Dean of Education, Faculty of Information Technology and Electrical Engineering. He was an IAS Visiting Professor with Yokohama National University, from 2016 to 2018. He has published around 250 international journals and conference papers. He holds six patents. He is also a coauthor of a book *Wireless UWB Body Area Networks: Using the IEEE802.15.4-201* (Elsevier/Academic Press) and a co-editor of book *UWB: Theory and Applications* (Chichester, U.K.: Wiley & Sons, Ltd., 2004). His research interests include future wireless communication systems, transceiver algorithms, and medical ICT. He has supervised 17 Ph.D. theses and more than 60 master's theses. He has been a Technical Program Committee (TPC) Member of about 25 conferences. He was the TPC Co-Chair of the IEEE PIMRC'2006, the TPC Chair of the ISMICT2007, the General Co-Chair of the ISMICT2011 and ISMICT2014, and the TPC Program Track Co-Chair of BodyNets 2012, PIMRC 2014, and PIMRC 2020, as well as the TPC Co-Chair of BodyNets 2018. He was also an Organizer of FEELIT 2008 and FEELIT 2011, and UWBAN2012, in 2013 and 2014, respectively. He serves as the Steering Committee Co-Chair of ISMICT series.